Journal of The Electrochemical Society, **159** (8) H722-H727 (2012)
0013-4651/2012/159(8)/H722/6/$28.00 © The Electrochemical Society

TiO_2 Nanowires on Anodic TiO_2 Nanotube Arrays (TNWs/TNAs): Formation Mechanism and Photocatalytic Performance

Ming-Yi Hsu, Hsin-Ling Hsu, and Jihperng Leu[*,z]

Department of Materials Science and Engineering, National Chiao Tung University, Hsinchu 30049, Taiwan

TiO_2 nanowires connected directly with TiO_2 nanotubes arrays (TNWs/TNAs) were successfully fabricated with a mixture of ethylene glycol and water that contained NH_4F electrolyte via a one-step method without mechanical stirring. The morphology of the TNWs/TNAs structure was investigated by changing the anodizing voltage and processing time to elucidate its formation mechanism. Well-developed anodic oxide nanowires are only observed under specific anodizing voltage and processing time conditions. The evolution of TNWs follows four stages: (1) thinning of the tube wall thickness with high roughness near the TNA mouths, (2) forming strings of through holes in the upper section of the TNAs, (3) splitting into nanowires, and (4) collapsing and further thinning of nanowires. For photocatalytic application, TNWs/TNAs film demonstrated a better photocatalytic performance than regular TNAs due to higher surface area predominantly and improved charge transport. Moreover, TNWs/TNAs film (20 nm wire/40 nm pore diameter) achieved a performance comparable to that of the film made from TiO_2 nanoparticles.
 [DOI: 10.1149/2.063208jes]

Manuscript submitted April 23, 2012; revised manuscript received May 29, 2012. Published July 20, 2012.

Since the first report on electrochemical photolysis of water at titanium dioxide (TiO_2) electrodes by Fujishima and Honda,[1] extensive research has shown that TiO_2 is an excellent material for the photodegradation of organic pollutants in water.[2–5] The TiO_2 layer is typically a nanocrystalline film comprised of a three dimensional network of interconnected nanoparticles of ∼20 nm size.[6] The large surface area associated with such films enables efficient light harvesting that in turn maximizes the amount of photogenerated charge. However, the structural disorder at the contact between two crystalline nanoparticles, may reduce electron mobility and hinder the charge separation efficiency,[7] thus diminishing the performance of nanoporous crystalline electrodes.

To achieve higher charge carrier transport than the nanoparticles, various forms of TiO_2 nanostructure, such as nanorods, nanowires, and nanotubes have attracted significant research interests in recent years.[8] Several studies have reported that one dimensional (1D) nanostructures can improve the charge-collection efficiency by promoting faster transport and slower recombination due to its axial transport path, compared to the random transport path in nanoparticles.[9] TiO_2 nanotube arrays (TNAs) grown by electrochemical anodization method was first reported by Zwilling et al.[10] with a length up to 500 nm (10:1 aspect ratio) using HF-based aqueous electrolyte. Several neutral electrolytes such as ethylene glycol (EG) or ammonium fluoride (NH_4F), have been employed to prepare anodized TiO_2 nanotubes with a higher aspect ratio.[11,12] Specifically, high aspect ratio (100:1), self-organized TiO_2 nanotubes have been produced using EG solution.[12] However, most of studies have been dedicated to one specific type of 1D TiO_2 structures such as nanotubes, nanorods, or nanowires, with less research on 1D TiO_2 hybrid structures. Recently, Turkevych et al.[13] fabricated a TiO_2 hybrid nanostructure with hierarchical morphology in the form of brush nanostructures by electrochemical anodization of Ti nanorods. In addition, Lim and Choi[14] demonstrated the TiO_2 nanowires directly connected TiO_2 nanotubes arrays structure (designated as TNWs/TNAs) using EG and NH_4F under mechanical stirring and proposed a bamboo-splitting model. Moreover, Wang et al.[15] used a TNWs/TNAs hybrid structure, prepared by anodization and a hydrothermal two-step method, for application in dye-sensitized solar cells (DSSCs). The DSSCs with such TiO_2 hybrid structure exhibited higher photovoltaic parameters and a lower dark current.[15] Yet, the details of the formation mechanism for TNWs/TNAs still need to be clarified. Also, little work has been reported on the applications of TNWs/TNAs and TNAs for their photocatalytic properties.

This study proposes a one-step method for the fabrication of a TNWs-covered TNAs (TNWs/TNAs) hybrid structure, using a mixture of EG and water containing NH_4F electrolyte without mechanical stirring. The morphology of the TNWs/TNAs structure was then examined by changing the anodizing voltage and processing time, to elucidate the detailed formation mechanism of TNWs/TNAs. The photocatalytic degradation of methylene blue (MB) using various TNWs/TNAs and TNAs structures was investigated and compared with the film made of TiO_2 nanoparticles.

Experimental

Fabrication and characterization of TiO_2 films.— Titanium foil (99.9% purity, 0.5 mm thickness) was used as the substrate for forming a TiO_2 layer by anodic oxidation. Prior to anodization, Ti foil was ultrasonically cleaned by distilled water, rinsed by acetone, and then dried by a purging N_2 gas. TiO_2 nanotube arrays and nanowires were fabricated at room temperature (25°C) by using electrolytes, consisting of ethylene glycol and water (99:1 in wt%) with 0.5 wt% NH_4F in a two-electrode configuration with a stainless steel foil (SS304) as a counter electrode at a constant DC potential. The process conditions of anodizing voltage and processing time were selected to elucidate the formation mechanism of TNWs/TNAs structures. First, the anodizing voltage was varied from 20 to 80 V, while the processing time was maintained at 1 h. Then, an anodizing voltage of 40 V was used, while the anodization time was increased from 30 min to 120 min. After fabrication of the TNWs/TNAs, thermal annealing was performed in ambient air at 450°C for 2 h, at a heating rate of 2°C/min. The surface and cross-section morphology of the TNAs were examined using a field emission scanning electron microscope (FESEM) (JOEL JSM-6700), which was operated at an accelerating voltage of 15.0 kV, and a focused ion beam scanning electron microscope (FIB/SEM) (FEI Nova-200), which was operated at an accelerating voltage of 5.0 kV. The surface areas of the TNWs/TNAs films were measured by dye (N719 dye, Solaronix) adsorption, which is a commonly used method in DSSC applications.[16] Specifically, the amount of dye adsorption was determined by desorbing the dye from the TiO_2 films into 5mM NaOH aqueous solution. The quantification was based on the dye's maximum absorption values at 515 nm in the dye-desorbed NaOH solutions as measured by an UV-visible light spectrometer (Evolution 300), using a dye solution of concentration 8×10^{-5} M as a reference.

Photocatalytic reaction experiments.— For the photocatalytic reaction experiments, the TNWs/TNAs film on Ti substrate of 2×1 cm^2 size was immersed in a quartz cuvette containing 10 mL methylene blue (MB) ($C_{16}H_{18}ClN_3S$, Acros Organics) solution with an initial concentration of 2.5×10^{-5} M. The samples were then irradiated by UV light at 360 nm using an 8W HeCd lamp (Sankyo Denki Co., Japan). The decomposition rate of the MB in the solution along with TNWs/TNAs films, can be obtained by monitoring its absorbance periodically (every 4 h) using an UV/Vis spectrometer at

*Electrochemical Society Active Member.
zE-mail: jimleu@mail.nctu.edu.tw

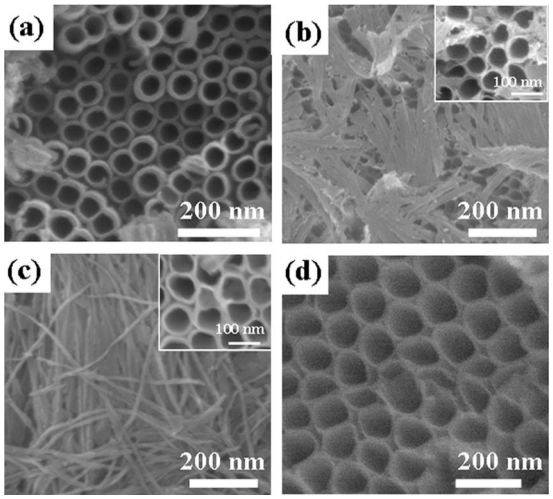

Figure 1. Surface morphology of the TiO_2 films prepared by anodic oxidation under different anodizing voltages: (a) 20 V, (b) 40 V, (c) 60 V, and (d) 80 V, with a constant anodizing time of 1 h.

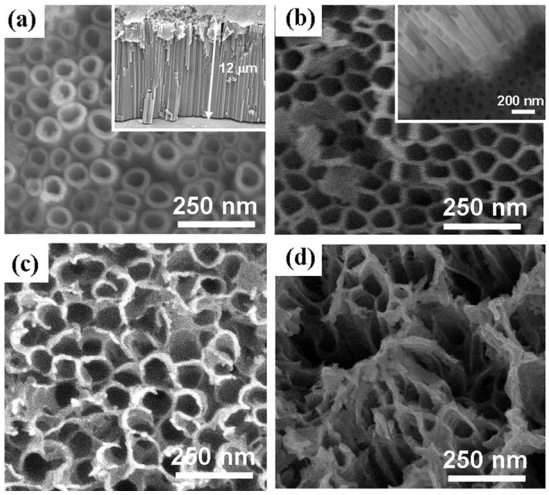

Figure 2. Surface morphology of the TiO_2 films prepared by anodic oxidation under different anodizing time: (a) 30 min, (b) 35 min, (c) 38 min, and (d) 40 min., with a constant anodizing voltage of 40 V.

wavelength 650 nm. The total height of the TNAs, TiO2 nanoparticles and TNWs/TNAs were maintained at 12 ± 0.5 μm, in which the TNAs tube length of TNWs/TNAs was ∼11 μm and the TNWs was ∼1 μm in cross-section with a wire length of ∼5-10 μm.

Results and Discussion

Influence of anodization parameters.— Figures 1a-1d illustrate the SEM images of the TiO_2 films prepared by various anodizing voltages from 20 V to 80 V, in a 0.5 wt% NH_4F solution with a constant anodizing time of 1 h. At anodizing voltage of 20 V shown in Fig. 1a, the surface morphology showed highly ordered TiO_2 nanotube arrays with a tube diameter (i.e. inner wall diameter) of 40 nm and a wall thickness of 20 nm. When the anodizing voltage was increased to 40 V, instead of highly ordered TNAs, TNWs appeared on the top surface with a wire width ∼50 nm. For the TiO_2 nanotubes beneath the TNWs, a diameter of 60 nm and a wall thickness of ∼10 nm was observed. As the anodizing voltage was further increased to 60 V, the entire surface was covered by TNWs with a width ∼20 nm on the TNAs with a diameter of 80 nm and a wall thickness of ∼10 nm TNAs. When the anodizing voltage was raised to 80 V, strikingly, there were no nanowires on the surface, only highly ordered TNAs with a diameter of ∼110 nm.

In order to understand the formation mechanism of TNWs/TNAs, the evolution of TiO_2 film was observed for a fixed anodizing voltage of 40 V and varyed anodizing times, from 30 to 120 min. Figures 2a-2d show the SEM images for the surface morphology of TiO_2 films prepared under a constant anodizing voltage of 40 V using an anodizing time of 30, 35, 38, and 40 min, respectively. For an anodizing time of 30 min, the length of the highly ordered TNAs structure was 12.2 μm, as shown in the inset of Fig. 2a; the TNAs structure possesses a tube diameter of 60 nm and a wall thickness of 18 nm. Up to 30 min, the steady-state growth rate of the TNAs length is approximately 0.4 μm/min. This suggests that high H^+ concentration is maintained at the pore bottom during chemical drilling[17] because the high-viscosity EG electrolyte limits the ionic diffusion of the electrolyte with a protective environment maintained along the pore walls and at the pore mouth during chemical drilling.

When the anodizing time was further increased to 35, 38, and 40 min as illustrated in Figs. 2b to 2d, a gradual change of the surface morphology near the top of the TNAs was observed. As the treatment time was increased from 30 to 35 min, the wall thickness was reduced from 18 nm (Fig. 2a) to 12 nm (Fig. 2b) due to the high electrochemical etching rate near the top of the TNAs. However, near the intermediate section of nanotubes, the wall thickness of the TNAs remained the same, ∼18 nm, as shown by the inset of Fig. 2b. This implies that enhanced electrochemical etching occurs near the top of the nanotube mouths, relative to the tubes in the intermediate section. As the treatment time was further increased to 38 and 40 min, as illustrated in Figs. 2c and 2d, the wall thickness became even thinner and the tubes started disintegrating in this transitional stage. After 45 min (Fig. 3(a1)), some of the TNAs near the top surface were broken up, along with the thinning of wall thickness down to about 10 nm. Further increasing the treatment time to 60 min, as illustrated by Fig. 3(b1), TNWs with a wire width of ∼50 nm were found on the entire surface. The nanowires then fell down on the top of the TNAs when its length became too long (∼2 μm). When the treatment time was increased up to 90 and 120 min (Figs. 3(c1) and 3(d1)), the TNWs completely covered on the top of the TNAs. The width of TNWs also decreased from 50 nm (after 60 min) down to ∼30 nm (after 90 min), then to ∼20 nm (after 120 min), due to chemical etching. Moreover, from the cross-section images illustrated in the right column of Fig. 3(a2) to 3(d2), the individual thicknesses of TNWs and TNAs layers in the TNWs/TNAs structure showed a different trend after the emergence of nanowires. The structure of the TNWs/TNAs with an anodizing time of 45 min showed two different zones in the cross-section image. At 45 min, the top layer's (partially TNWs and mostly TNAs in the transitional stage) thickness was ∼2 μm, and the thickness of the TNAs was ∼10 μm. After 60 min, the structure collapsed into ∼1 μm thickness of nanowires after splitting of the tubes, and the thickness of the TNAs maintained at 10 μm as shown in Fig. 3(b2). However, the thickness of TNWs did not change with time and remained at about 1 μm on the top surface. As the anodizing time was further increased to 90 and 120 min, the nanowire structure emerged upon further etching, whereas the length of the TNAs was increased to 11 μm (after 90 min; Fig. 3(c2)) and 12 μm (after 120 min; Fig. 3(d2)). A top-view of the TNWs, as illustrated in Fig. 3(d3), showed that the length of nanowires was 5-10 μm with excellent coverage.

Both the strength of the electric field and the processing time play important roles in the formation of TNWs/TNAs. Figure 4a summarizes the conditions of required anodizing voltage and processing time for forming TNWs/TNAs in a fixed electrolyte solution. For instance, TNWs/TNAs emerged after 120 min treatment at 30 V, but only 30 min for anodizing voltage of 50–60 V. To elucidate the influence of the electric field strength on the TNWs/TNAs, ion migration under electric field in the electrolyte shall be taken into consideration. In principle, the flux of ions in the presence of electric field can be expressed as:

$$J_i = -D_i \frac{\partial c_i}{\partial x} - u_i c_i E \qquad [1]$$

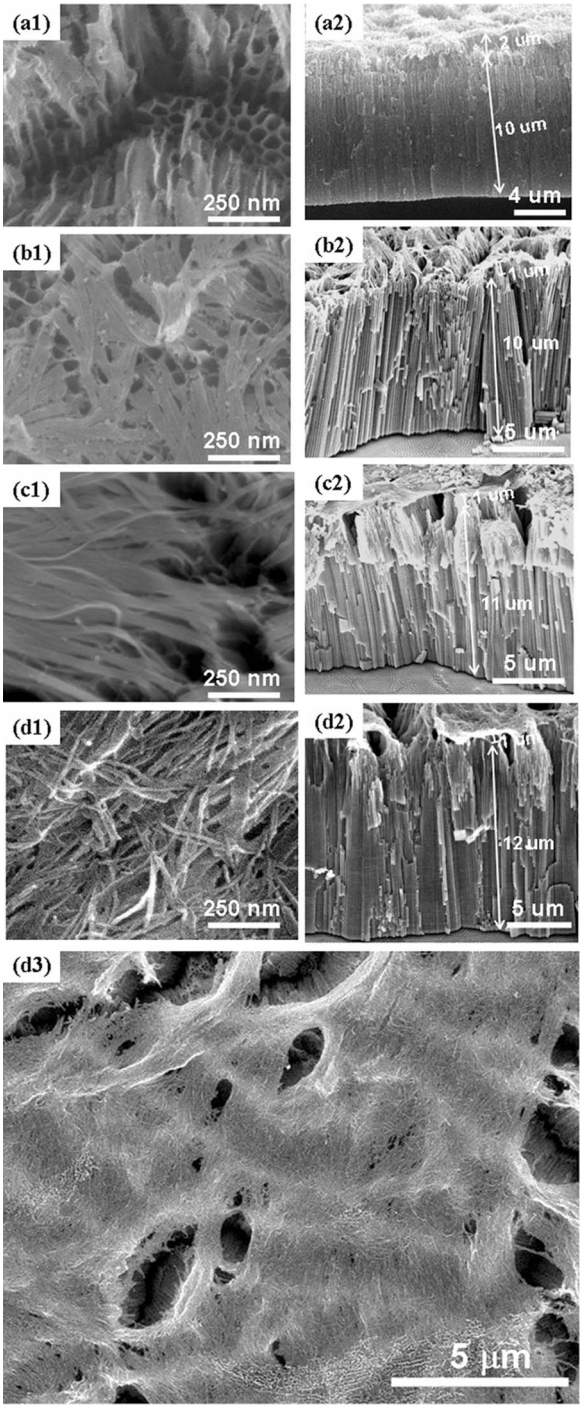

Figure 3. Surface (1) and cross-section (2) morphologies of the TiO_2 films prepared by anodic oxidation at different anodizing time: (a) 45 min, (b) 60 min, (c) 90 min, and (d) 120 min, with a constant anodizing voltage of 40 V; (d3) Surface morphology at low magnification.

where J_i is the flux of species i of concentration c_i in direction x, $\frac{\partial c_i}{\partial x}$ is the concentration gradient, D_i is the diffusion coefficient, u_i is the mobility of species i, and E is the electric field strength. Evidently, ion transport in the electrolyte is significantly affected by field strength, since ion migration within the electric field is considerable in comparison to the process of ion diffusion under a concentration gradient. According to Eq. 1, higher field strength results in higher ion flux in the electrolyte. As a result, under high field strength, the TNWs/TNAs structure formed in a shorter time. However, TNWs emerges only under anodizing voltage of 30 to 60 V with longer processing times for lower voltages.

To understand the controlling factor(s) for the formation of nanowires onto TNAs, the pore diameter and the wall thickness of TNAs top section prior to the emergence of nanowires, as a function of voltage were quantified by SEM are shown in Fig. 4b. For cases with no TNWs formation, for example, at $\leq$20 V or $\geq$80 V, the tube diameter and wall thickness were taken from TNAs after a processing time of 30 min. The pore diameter of the TNAs mouth increased from 30 to 110 nm with increasing applied voltage from 10 to 80 V, which agreed with the reported results.[18–20] However, the wall thickness of the TNAs mouths decreased from 20 nm to 8 nm as the applied potential was raised from 10 to 80 V. In particular, TNWs/TNAs occur only when the tube wall thickness at the mouths is between 15 and 10 nm. From Figs. 4a and 4b, it is clear that if the applied voltage was too low, the lower dissolution rate could not break up TiO_2 tube wall, but retained the TNAs structure as function of time. In contrast, at specific voltages, in which the wall thickness at the tube mouth is ~10 nm, the areas of thinner wall near the top of TNAs because of the high thickness non-uniformity from roughness, would be etched through and form the nanowires. A detailed formation mechanism will be proposed in the subsequent section. By contrary, if the anodizing voltage was too high together with a thin wall thickness of ~8 nm, TiO_2 tube wall of top section would be completely removed, resulting in shortened TiO_2 nanotube arrays without nanowires.

Formation mechanism of TNWs/TNAs.— Based on above results, TiO_2 nanowires are found to evolve and form on the top of TNAs through several stages. Figures 5a-5d show the schematic diagrams along with their corresponding surface morphology SEM images for four key stages in the TNWs/TNAs formation mechanism. First, as the anodic titanium oxide reaction began, the ordered TNAs was formed, resulting from the field-enhanced chemical drilling by a high H^+ concentration at the pore bottom of the tubes, in conjunction with a protective environment maintained along the pore walls by the highly viscous EG solution, as described in the previous section. As the anodic oxidation reaction proceeded, field-enhanced dissolution in the tube bottom still prevailed to further increase the aspect ratio (height/diameter) of the TNA at this stage, as illustrated in Fig. 5a. However, the wall thickness near the tube mouth shown in Fig. 5a, became smaller due to enhanced dissolution of TiO_2. In the EG/H_2O solution containing NH_4F electrolyte, the migration of F^- toward the electric field of the bottom electrode, is inhibited by the highly viscous solution. This results in F^- concentration much higher at the tube mouth than at the tube bottom.[21] With the presence of water in our case, the hydrogen ions further enhance the chemical dissolution reaction of the formed TiO_2 tube:[22]

$$TiO_2 + 6F^- + 4H^+ \rightarrow TiF_6^{2-} + 2H_2O \qquad [2]$$

Therefore, the tube wall thickness near the tube mouth was thinner than the lower sections as illustrated in Fig. 5a.

Meanwhile, the inner surface of the tubes was rough, as reported by Liu et al.,[23] because mechanical stirring in the electrolyte bath was not used in this study. Thus, the inner tube diameter of the TNAs was not uniform, as schematically illustrated in the inset 1 of Fig. 5b and marked by arrows. Under a specific voltage and processing time conditions, in which the wall thickness at the tube mouth is < 10 nm, the areas of thinner wall thickness near the top of the TNAs would be etched through by the enhanced TiO_2 dissolution reaction as illustrated in inset 2. With increasing processing time, strings of through holes on the tubes in the top section of the TNAs, were formed from top to bottom, along the F^- ion migration direction under electric field, as illustrated in Fig. 5b.

As the TiO_2 dissolution reaction continued over time, the strings of through holes on the tube wall would initiate and propagate downward, while the holes near the top expanded and became connected to split into nanowires, as illustrated in Fig. 5c. With increasing anodizing time, the nanowires were further chemically etched, resulting in

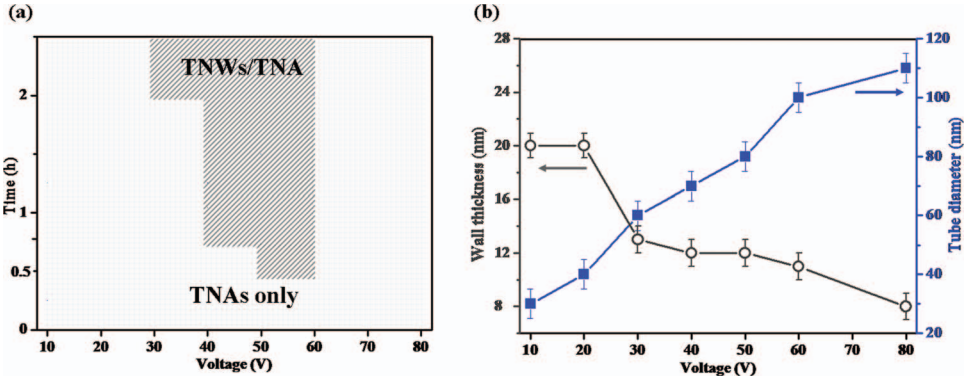

Figure 4. (a) Conditions of required anodizing voltage and processing time (shaded zone) for forming TNWs/TNAs. (b) The pore diameter and wall thickness of TNAs top section prior to the emergence of nanowires, as a function of voltage. For cases without TNWs formation, a processing time of 30 min was used.

smooth wire edge and narrower wire width of nanowires. In addition, the nanowires would collapse onto the TNAs when its length is ~5-10 μm, as illustrated in Fig. 5d. In summary, a strings-of-through-holes model is proposed, based on the enhanced TiO_2 dissolution reaction near the top section in conjunction with a threshold wall thickness of ~10 nm for forming nanowires and high thickness non-uniformity due to a lack of mechanical stirring. Four key stages in the TNWs/TNAs formation mechanism are: (a) thinning of the tube wall thickness with high roughness near the TNAs mouths, (b) forming strings of through holes in the top section of the TNAs, (c) splitting into nanowires, and (d) collapsing and further thinning of nanowires.

Photocatalytic performance.— Our attention then shifted to the photocatalytic performance of TNWs/TNAs nanostructure. The effect of various TiO_2 morphologies including ordered TNAs and TNWs/TNAs on the photocatalytic degradation of methylene blue (MB) was examined and compared with that of TiO_2 film made of TiO_2 particles. In order to compare the photocatalytic performance of pure TNAs and TNWs/TNAs structures, we adjusted the process conditions (under mechanical stirring) to fabricate pure TNAs with diameters ranging from 40 to 100 nm with a total tube length or thickness of ~11 μm. Figure 6 shows the photodegradation of MB solution, C_t/C_o as a function of UV irradiation time for various anodized TiO_2 (TNAs and TNWs/TNAs) films and TiO_2 film of TiO_2 particles. It was found that MB degradation versus reaction time curves ($C_0 = 2.5\times10^{-5}$ M) follows a pseudo first-order kinetics as described by the Langmuir–Hinshelwood model.[24] Thus, the photodegradation rate of MB could be expressed by the following Eqs. 3 and 4:

$$C_t = C_0 e^{-kt} \quad [3]$$

$$\ln C_t/C_0 = -kt \quad [4]$$

where k is the apparent reaction rate constant, t is the irradiation time; C_0 and C_t are the initial concentration and the reaction concentration of MB. The reaction rate constants (k) were calculated from the experimental data using a linear regression. In all cases, correlation coefficients, R^2 values are all higher than 0.95, indicating that the Langmuir–Hinshelwood model can well describe the kinetics of MB degradation.

For the TNAs structures with various tube diameters as shown in Fig. 6, the corresponding k values are 9.80×10^{-2} h^{-1}, 8.48×10^{-2} h^{-1}, 6.73×10^{-2} h^{-1} and 5.49×10^{-2} h^{-1} for tube diameter of 40 nm, 60 nm, 80 nm, and 100 nm, respectively. A higher reaction rate was observed for TNAs with a smaller tube diameter at a fixed tube thickness.

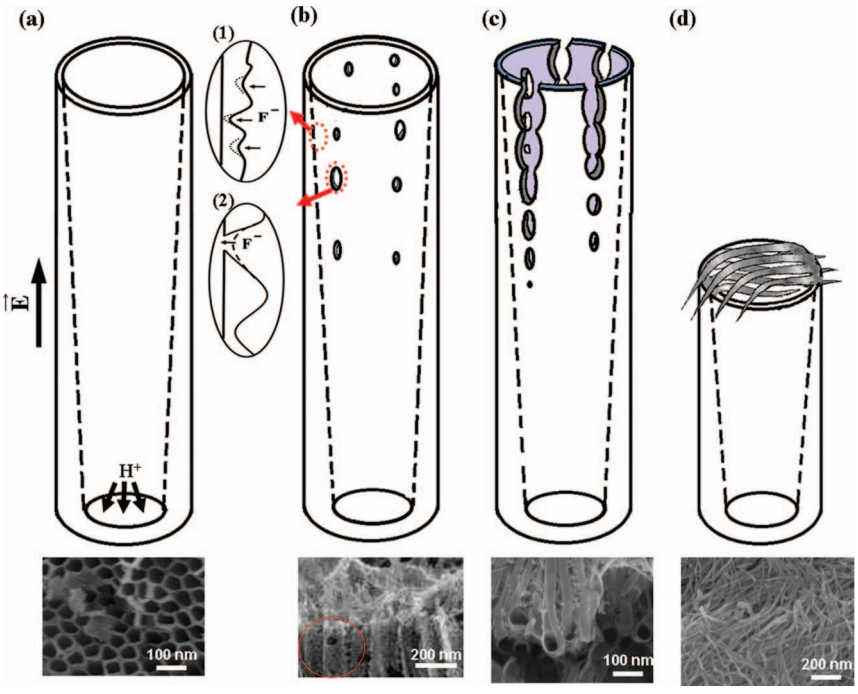

Figure 5. Schematic diagrams along with their corresponding surface morphology SEM images for four key stages in the TNWs/TNAs formation mechanism: (a) thinning the tube wall thickness with high roughness near the TNAs mouths, (b) forming strings of through holes in the top section of TNAs, (c) splitting into nanowires, and (d) collapsing and further thinning of nanowires.

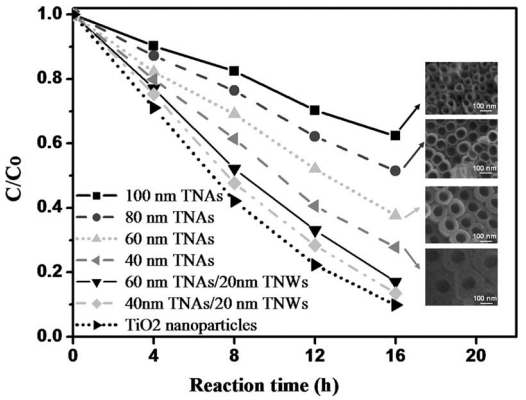

Figure 6. Photocatalytic degradation of MB under UV light irradiation, (C/C_o) vs. reaction time plots for various TNAs, TNWs/TNAs, and TiO_2 nanoparticles films.

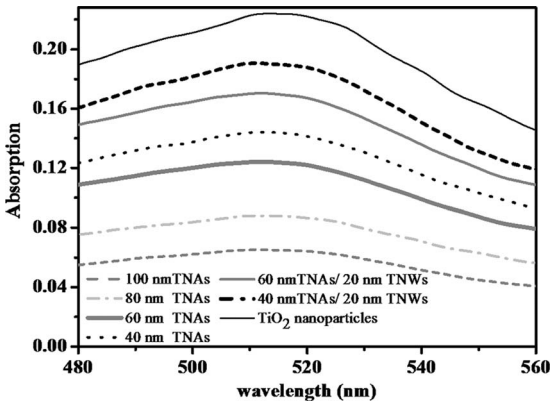

Figure 7. UV-visible spectra of the desorbed dye from the solution of various TNAs, TNWs/TNAs, and TiO_2 nanoparticles films.

In comparison, for fixed TNAs with 60 nm tube diameter, the rate constant, k for 20 nm TNWs/60 nm TNAs is 12.54×10^{-2} h^{-1}, which is 48% higher than that of pure TNAs (8.40×10^{-2} h^{-1}). For fixed TNAs with 40 nm tube diameter, the rate constant, k for 20 nm TNWs/40nm TNAs is 13.05×10^{-2} h^{-1}, which is 33% higher than that of pure TNAs (9.80×10^{-2} h^{-1}). In short, the TNWs/TNAs film exhibited 33-48% higher photocatalytic activity than their corresponding pure TNAs.

The role of surface on the enhanced photocatalytic performance of TNWs/TNAs is first examined. Since the conventional Brunauer–Emmett–Teller (BET) method[25] is not suitable for measurement of the surface area of various TiO_2 films, the dye desorption amount, an indicator of surface area, was measured by UV-visible spectrum. From the spectra data, the dye adsorption of a TiO_2 film could be calculated by comparing the light absorption intensity of dye-desorbed NaOH solution. In addition, the Beer-Lambert law, as expressed by Eqs. 5 and 6, is applied to calculate the dye adsorption amount within various TiO_2 films.

$$T = \frac{I}{I_0} = 10^{-\alpha.l} = 10^{-\varepsilon.c.l} \quad [5]$$

$$A = -\log\left(\frac{I}{I_0}\right) = \varepsilon cl \quad [6]$$

where T is light transmittance, I is the absorption intensity, α is the absorption coefficient, l is the sample thickness, c is the concentration, ϵ is the extinction coefficient, and A is light absorption.

The absorbance intensity at 515 nm wavelength of a reference solution with dye concentration 8×10^{-5} M was 0.521. Using Eq. 6, the concentration of the solution, i.e. the dye adsorption on TiO_2 films, can be obtained by taking the hybrid film thickness (12 μm) into account. Fig. 7 shows the UV-visible spectra of the dye desorbed to NaOH solutions for TNAs, TNWs/TNAs, and TiO_2 nanoparticle films. In addition, the calculated dye adsorption, and reaction rate constants (k) of various TiO_2 films are summarized in Table I. From Fig. 7 and Table I, the dye adsorption of various pure TNAs films shows that a smaller tube diameter yields higher adsorption intensity. This means that TNA with a smaller tube diameter possesses has a higher surface area, which results in enhanced photocatalytic efficiency. For TNWs/TNAs films, the adsorption intensity, i.e. surface area, is higher than that for corresponding TNAs film. It is believed that the large surface area of the TiO_2 film enhances the adsorption of pollutants and enables light harvesting with a higher amount of photo-generated charge.[26] For pure TNAs, the difference in surface area comes from different tube density of anodic TNAs films. As the anodizing voltage increased, the tube density decreased with increasing tube diameter. In turn, the amount of dye adsorption decreased, leading to a reduced photocatalytic efficiency.

Meanwhile TNWs/TNAs structure had a higher photocatalytic efficiency than pure TNAs, which can be also attributed to the higher surface area of the nanowires. Dye adsorption data (Fig. 7) shows that TNWs/TNAs had higher adsorption intensity. Therefore, the congregation of the bundled nanowires connected to the nanotube mouths had a higher surface area than the nanotubes. Conversely, compared the change percentage between dye adsorption data and reaction rate constants, all the TNAs and TNWs/TNA films get higher reaction rate than dye adsorption data. This may be due to the fact that not only surface area, a predominant factor, but also charge transport or reduced recombination may also affect the photocatalytic performance, because the directly connected 1D nanostructures of the TNAs and TNWs/TNA may improve the charge-collection efficiency by promoting faster transport and slower recombination. This was helpful for faster transport and slower recombination to the random transport path in nanoparticles.[27] Overall, the photocatalytic performance (k value $= 13.05\times10^{-2}$ h^{-1}) of TNWs/TNA on a Ti plate used in this study has achieved a very high efficiency, close to that of TiO_2 nanoparticles (k value $= 14.38\times10^{-2}$ h^{-1}). However, photocatalysis of pollutants in an immobilized film form, such as TNAs or TNWs/TNAs hybrid structure, is more practical than that in a TiO_2 powdery form. It is believed that the performance can be further improved by optimizing the width and density of the nanowire for a fixed TNAs structure.

Table I. Dye adsorption, reaction rate constants (k), and change percentage of various TiO_2 films.

TiO_2 film	Dye Adsorption ($\times10^{-8}$ mol/cm^2)	change% relative to nanoparticles	reaction rate constants, k ($\times10^{-2}$ h^{-1})	change% relative to nanoparticles
100 nm TNAs	1.22	29%	5.49	38%
80 nm TNAs	1.65	39%	6.73	47%
60 nm TNAs	2.33	55%	8.48	59%
40 nm TNAs	2.72	64%	9.80	68%
60 nm TNAs/ 20 nm TNWs	3.21	76%	12.54	87%
40 nm TNAs/ 20 nm TNWs	3.58	85%	13.05	91%
TiO_2 nanoparticles	4.22	100%	14.38	100%

Conclusions

This study demonstrates one-step process for the formation of TNWs/TNAs structure by anodization of Ti foils in a mixture of ethylene glycol and water containing NH_4F electrolyte without mechanical stirring. A formation mechanism for TNWs/TNAs is proposed and examined by changing the anodizing time and voltage. The evolution of TNWs/TNAs growth first involves thinning the tube wall thickness with high roughness and forming strings of through holes in the top section of the TNAs, due to enhanced dissolution of TiO_2 by the high F^- concentration and presence of H^+ from water. Then the strings of through holes on the tube wall initiate and propagate downward. Finally, the holes near the top expand and connect to split into nanowires. The TNWs/TNAs demonstrate superior photocatalytic ability, because of the congregation of the bundled nanowires connected to the nanotube mouths, which increases the surface area, a predominant factor, and the TNWs directly connected on nanotubes gains an advantage to retard the charge recombination of the electron and hole pairs.

Acknowledgments

The authors appreciate the financial support by National Science Council of ROC under contract numbers: NSC 101-2221-E-009-126-MY2 and NSC 101-3113-E-007-001.

References

1. A. Fujishima and K. Honda, *Nature*, **238**, 37 (1972).
2. D. Jiang, S. Zhang, and H. Zhao, *EnViron. Sci. Technol.*, **41**, 303 (2007).
3. Z. Y. Liu, X. T. Zhang, S. Nishimoto, M. Jin, D. A. Tryk, T. Murakami, and A. Fujishima, *J. Phys. Chem. C*, **112**, 253 (2008).
4. X. Wang, H. M. Zhao, X. Quan, Y. Z. Zhao, and S. Chen, *J. Hazard. Mater.*, **166**, 547 (2009).
5. Y. Liu, J. Li, B. Zhou, J. Bai, Q. Zheng, J. Zhang, and W. Cai, *Environ. Chem. Lett.*, **7**, 363 (2009).
6. M. Grätzel, *J. Photochem. Photobiol. A*, **164**, 3 (2004).
7. T. Y. Peng, A. Hasegawa, J. R. Qiu, and K. Hirao, *Chem. Mater.*, **15**, 2011 (2003).
8. Y. Alivov and Z. Y. Fan, *Appl. Phys. Lett.*, **95**, 063504 (2009).
9. G. K. Mor, K. Shankar, M. Paulose, O. K. Varghese, and C. A. Grimes, *Nano Lett.*, **6**, 215 (2006).
10. V. Zwilling, E. Darque-Ceretti, A. Boutry-Forveille, D. David, M. Y. Perrin, and M. Aucouturier, *Surf. Interface Anal.*, **27**, 629 (1999).
11. J. M. Macak, H. Tsuchiya, L. Taveira, S. Aldabergerova, and P. Schmuki, *Angew. Chem., Int. Ed.*, **44**, 7463 (2005).
12. M. Paulose, K. Shankar, S. Yoriya, H. E. Prakasam, O. K. Varghese, G. K. Mor, T. A. Latempa, J. A. Fitzgerald, and C. A. Grimes, *J. Phys. Chem. B*, **110**, 16179 (2006).
13. I. Turkevych, Y. Pihosh, K. Hara, Z. S. Wang, and M. Kondo, *Jpn. J. Appl. Phys.*, **48**, 06FE02 (2009).
14. J. H. Lim and J. Choi, *Small*, **3**, 1504 (2007).
15. Y. Wang, H. X. Yang, and H. Xu, *Mater. Lett.*, **64**, 164 (2010).
16. K. Fan, M. Liu, T. Peng, L. Ma, and K. Dai, *Renewable Energy*, **35**, 555 (2010).
17. J. M. Macak, H. Tsuchiya, and P. Schmuki, *Angew. Chem., Int. Ed.*, **44**, 2100 (2005).
18. S. Bauer, S. Kleber, and P. Schmuki, *Electrochem. Commun.*, **8**, 1321 (2006).
19. I. Paramasivam, J. M. Macak, T. Selvam, and P. Schmuki, *Electrochim. Acta*, **54**, 643 (2008).
20. Y. Yang, X. Wang, and L. Li, *J. Am. Ceram. Soc.*, **91**, 3086 (2008).
21. L. Sun, S. Zhang, X. W. Sun, and X. He, *J. Electroanal. Chem.*, **637**, 6 (2009).
22. H. Yin, H. Liu, and W. Z. Shen, *Nanotechnology*, **21**, 035601 (2010).
23. H. Liu, L. Tao, and W. Shen, *Nanotechnology*, **22**, 155603 (2011).
24. S. D. Sharma, K. K. Saini, C. Kant, C. P. Sharma, and S. C. Jain, *Appl. Catal. B*, **84**, 233 (2008).
25. S. Brunauer, P. H. Emmett, and E. Teller, *J. Am. Chem. Soc.*, **60**, 309 (1938).
26. D. S. Kima and S. Y. Kwak, *Appl. Catal. A*, **323**, 110 (2007).
27. K. Zhu, N. R. Neale, A. Miedaner, and A. J. Frank, *Nano Lett.*, **7**, 69 (2007).